



## OPEN ACCESS

## EDITED BY

Irene Taurino,  
KU Leuven, Belgium

## REVIEWED BY

Alessandra Quarta,  
National Research Council (CNR), Italy  
Ahmed Alsadig Ahmed Mohammed,  
National Research Council (CNR), Italy

## \*CORRESPONDENCE

Valentina Marassi,  
✉ valentina.marassi@unibo.it

<sup>†</sup>These authors contributed equally to this work and share first authorship

## SPECIALTY SECTION

This article was submitted to Lab-on-a-Chip Devices, a section of the journal Frontiers in Sensors

RECEIVED 02 November 2022

ACCEPTED 01 December 2022

PUBLISHED 15 December 2022

## CITATION

Wang J, Giordani S, Marassi V, Roda B, Reschiglian P and Zattoni A (2022), Quality control and purification of ready-to-use conjugated gold nanoparticles to ensure effectiveness in biosensing. *Front. Sens.* 3:1087115. doi: 10.3389/fsens.2022.1087115

## COPYRIGHT

© 2022 Wang, Giordani, Marassi, Roda, Reschiglian and Zattoni. This is an open-access article distributed under the terms of the [Creative Commons Attribution License \(CC BY\)](https://creativecommons.org/licenses/by/4.0/). The use, distribution or reproduction in other forums is permitted, provided the original author(s) and the copyright owner(s) are credited and that the original publication in this journal is cited, in accordance with accepted academic practice. No use, distribution or reproduction is permitted which does not comply with these terms.

# Quality control and purification of ready-to-use conjugated gold nanoparticles to ensure effectiveness in biosensing

Junjie Wang<sup>1†</sup>, Stefano Giordani<sup>1†</sup>, Valentina Marassi<sup>1,2\*</sup>, Barbara Roda<sup>1,2</sup>, Pierluigi Reschiglian<sup>1,2</sup> and Andrea Zattoni<sup>1,2</sup>

<sup>1</sup>Department of Chemistry G. Ciamician, University of Bologna, Bologna, Italy, <sup>2</sup>ByFlow SRL, Bologna, Italy

**Introduction:** Gold nanoparticles (AuNPs) and their conjugates are used for many applications in the field of sensors. Literature lacks procedures able to separate, purify and characterize these species in native conditions without altering them while assuring a high throughput. This technological gap can be reduced by exploiting Asymmetrical Flow Field Flow Fractionation multidetection platforms (AF4 multidetection).

**Method:** This work describes a complete set of strategies based on the AF4 system, from nanoparticle synthesis to separative method optimization to conjugates screening and characterization, achieving quantitative control and purification of ready-to-use conjugated Gold nanoparticles and ensuring effectiveness in biosensing.

**Results and Discussion:** AF4-multidetection was used to study AuNPs with different types of surface coating [Poly ethylene glycol, (PEG) and Citrate], their binding behaviour with protein (Bovine serum albumin, BSA) and their stability after conjugation to BSA. A robust but flexible method was developed, able to be applied to different AuNPs and conjugating molecules. The morphology and conjugation mechanism of AuNPs-BSA conjugates were evaluated by combining online Multiangle light scattering (MALS) and offline Dynamic Light Scattering (DLS) measures, which provided an important feature for the quality control required to optimize bio-probe synthesis and subsequent bioassays.

## KEYWORDS

biosensor development, AuNPs, native separation, FFF-multidetection, protein conjugation

## 1 Introduction

Engineered metal nanoparticles have attracted a lot of interest due to their application in numerous fields such as catalysis, disease diagnosis and treatment, sensor technology, and labeling of optoelectronic recorded media. (Jamkhande et al., 2019). However, numerous reports reveal a series of drawbacks that limit their biochemical applications. For example, silver nanoparticles (AgNPs) have high toxicity to host cells while Pd Nanocrystals induce reactive oxygen species (ROS) formation. (Wang et al., 2020). The emergence of gold nanoparticles has largely filled this gap due to their outstanding features. Their physical properties make them good imaging enhancers for x-ray imaging and computed tomography, and they are easy to customize by simple surface modification, reaching excellent biocompatibility and high versatility. Their synthetic strategy allows to obtain a wide range of differently sized and shaped (nanoparticles, nanorods, nano stars, and nano shells) NPs. (Tian et al., 2017). The study of AuNPs-proteins interactions and characterization of the resulting species allowed the development of numerous optical assays, (Guarise et al., 2006; Chuang et al., 2010; Piovarci et al., 2021) while also representing a necessary requirements in the development of systems within applications in healthcare and food chemistry (Delong et al., 2010; Wimuktiwan et al., 2015). For example, label-free colorimetric sensors based on functionalized AuNPs with aptamers or proteins have been widely used due to their easy readout and potential for high throughput formats (Melikishvili et al., 2021; Zhang and Liu, 2021): in the presence of target analytes gold nanoparticles (AuNPs) are subjected to aggregation/de-aggregation processes generating an absorbance shift (due to plasmon resonance) which is able to reveal the presence of the target of interest. Therefore, it is crucial to create procedures that can purify and carry out a “quality check” on the NPs/conjugates in a fast way and with high throughput to ensure working with very narrow size distributions.

Various analytical techniques have been exploited to examine NPs, their conjugates, and associated properties. Examples are ultraviolet-visible spectroscopy, (Li et al., 2010) fluorescence spectroscopy, (Mariam et al., 2011) dynamic light scattering, (Dobrovolskaia et al., 2009) atomic force microscopy, (Deng et al., 2009) size exclusion chromatography (SEC), (Lundqvist et al., 2008) capillary electrophoresis (CE), (Boulos et al., 2013) steady state quenching titration, (Boulos et al., 2013) and circular dichroism. (Treuel et al., 2010). However, most of them work in batch mode and are able to only provide average results for the sample. While SEC and EC are able to separate (thus potentially purify) different components of a mixture (ex. AuNPs, proteins and conjugates), they are extremely limited in terms of mobile phase applicable. Moreover, these strategies often result in low sample recoveries. An improvement may be represented by the use of the highly flexible Asymmetrical Flow Field Flow Fractionation (AF4). AF4 is a non-destructive, native size-

based separation technique where the eluted fractions can be collected for further analysis (Marassi et al., 2019). AF4-multidetector platforms have proven themselves as powerful tools to analyze nanoparticles and metal nanoparticles, (Marassi et al., 2018a; Roda et al., 2018; Caputo et al., 2021; Marassi et al., 2022a) proteins and antibodies, (Qureshi and Kok, 2011; Leeman et al., 2018; Marassi et al., 2021a; Leeman et al., 2021) aptamers, (Ashby et al., 2014; Marassi et al., 2022b) even in complex matrixes. (Lee et al., 2018; Marassi et al., 2021b; Marassi et al., 2022c; Ventouri et al., 2022; Zappi et al., 2022). These platforms made it possible to see the aggregation process involved in binding experiments as well as to examine the binding behavior of various species to AuNP surfaces (Meisterjahn et al., 2014; Saenmuangchin and Siripinyanond, 2018). Additionally, these platforms enabled the separation of conjugates from free components as well as the characterization of their size, mass, and spectroscopic properties. The results also demonstrated the platform's adaptability in terms of mobile phase choice, enabling the tests to be carried out in the ideal setting for the conjugated system. A further improvement in AF4 characterization of these systems can be obtained by the coupling of the platform with an Inductively coupled plasma-mass spectrometry (ICP-MS) detector which provides lower Limit of detection (LODs) and allows powerful peak deconvolution to identify different coeluting species. (Bouzas-Ramos et al., 2019; López-Sanz et al., 2019; Marassi et al., 2022d). However, the cost of the detector and the fact the sample is destroyed upon analysis prevent the collection of the separated protein-AuNPs systems and is a drawback for application in the production pipeline.

Literature studies, also involving Field Flow Fractionation (FFF), focusing of the interactions between AuNPs and albumins are surprisingly limited considering their relevance in biological systems. (Tsai et al., 2011; López-Sanz et al., 2019). Moreover, little attention was paid to the effect of surface properties on binding behavior and protein abundance on the nanoparticle surface, which are extremely important for analytes quantification and their possible future applications.

The aim of this work is to apply an AF4 system combined with photodiode array and multiangle light scattering detector (AF4-DAD-MALS) for developing a complete and flexible analysis strategy of AuNPs with different surface coatings, namely PEG-AuNPs and Citrate- AuNPs. In particular, while PEG is also reported to prevent non-specific interactions of serum proteins with nanoparticles, (Free et al., 2009) there are also some reports where BSA was able to rapidly couple to PEG-encapsulated gold nanoparticles increasing their stability and biocompatibility and preventing aggregation, aspect strongly desired for any applications related to biosensors. (Boulos et al., 2013; Nicoară et al., 2019). Therefore, it is extremely necessary to further clarify their binding behavior of PEG-AuNPs and their coupling mechanism in biological or saline environments.

With this aim, we monitored the size evolution of synthesized AuNPs in water and application-like medium. Then, the method was optimized to characterize the different adsorption behavior of protein on their surface. Overall this approach can offer a powerful tool for the high-throughput production and characterization of NPs/conjugates for sensors applications: a careful experiment design allowed also for the first time to evaluate the mechanism of the protein coating by considering online sizing results, both overcoming Dynamic light scattering (DLS) limitation and providing compatible results with standard methods.

## 2 Materials and methods

### 2.1 Materials

Gold (III) chloride trihydrate ( $\text{HAuCl}_4 \cdot 3\text{H}_2\text{O}$ ,  $\geq 49.0\%$  Au basis), Sodium citrate ( $\text{C}_6\text{H}_5\text{Na}_3\text{O}_7$ ,  $\geq 98.0\%$ ), Sodium phosphate dibasic dihydrate ( $\text{Na}_2\text{HPO}_4 \cdot 2\text{H}_2\text{O}$ ,  $\geq 99.0\%$ ), Sodium phosphate monobasic dihydrate ( $\text{NaH}_2\text{PO}_4 \cdot 2\text{H}_2\text{O}$ ,  $\geq 99.0\%$ ), Poly(ethylene glycol) methyl ether thiol (5000 g/mol), and Bovine serum albumin (BSA,  $\geq 98.0\%$ ) were purchased by Sigma Aldrich (St. Louis, MO, United States of America). All AuNPs solutions were prepared with purified 18 M $\Omega$  water. Glassware was cleaned with aqua regia and rinsed thoroughly with deionized water.

### 2.2 Synthesis of gold nanoparticles (AuNPs)

Citrate AuNPs. The AuNPs were made utilizing a simple wet chemical process, as described in the previous literature. (Yang et al., 2016). In brief, 100 ml of  $\text{HAuCl}_4$  (1 mM) was heated to boiling, then 6 ml of freshly produced sodium citrate (38.8 mM) was promptly added to the boiling solution with vigorous stirring and held for 15–30 min. The color of the solution quickly changed from pale yellow to colorless, then to dark purple. The solution was constantly stirred at the end of this operation until it cooled to room temperature and was kept at 4°C.

Poly(ethylene glycol) (PEG)-AuNPs. The PEG-AuNPs were synthesized by decomposing citrate on the surface of the AuNPs with a thiolated Poly(ethylene glycol) (mPEG-SH). (Fernández-López et al., 2009). Briefly, 100 ml aqueous solution of as-prepared citrate AuNPs was concentrated to 10 ml *via* centrifugation. Following that, 2 ml of mPEG-SH (5000 g/mol) was added dropwise under vigorous stirring to 10 ml of as-synthesized citrate AuNPs. The mixture was left to react for 12 h. The PEG-capped particles were filtered and redispersed in water after centrifugation at 13,500 rpm for 20 min. The concentration of AuNPs in the solutions was determined by UV-vis spectrum (shown in supplementary). These measurements were conducted with a UV-2600i SHIMADZU UV-visible spectrophotometer (SHIMADZU, United Kingdom).

### 2.3 Synthesis of AuNPs-BSA conjugation

The AuNPs were conjugated with BSA through passive adsorption of proteins onto AuNPs surface as previously described. (Safenkova et al., 2010). Firstly, the AuNPs were diluted in water to 50  $\mu\text{g}/\text{ml}$ . Then, they were mixed 1:1 in volume with a 100  $\mu\text{g}/\text{ml}$  BSA solution in phosphate buffer (10 mM, pH 7.4), to obtain a final AuNP and BSA concentration of 25 and 50  $\mu\text{g}/\text{ml}$ , respectively. The mixture samples were incubated for 30 min and 48 h at room temperature (RT  $\sim 25^\circ\text{C}$ ). The conjugation reaction between BSA and AuNPs was verified by the UV-Vis spectral shift of wavelength at the maximum absorption. The size distribution test of AuNPs and their conjugates from Dynamic light scattering (DLS) with a red laser (633 nm), Zetasizer (Malvern Instrument Nano Series ZS, Worcestershire, United Kingdom). A disposable cell (DTS0012; Malvern Instruments, United Kingdom) was used for DLS measurements. The experimental parameters are as follows: measurements angle 173°, temperature 25°C, and each sample was collected at least three times. The data were collected and analyzed with Malvern Software ver. 7.13.

### 2.4 Asymmetrical flow field-flow fractionation (AF4) coupled with DAD detector, multi-angle laser light scattering (AF4-UV/vis -MALS)

The AF4 system used is an AF2000 Multiflow asymmetrical flow field flow fractionation system manufactured by Postnova Analytics (Germany) which contains a Postnova PN7520 solvent degasser, two Postnova PN1130 Isocratic Pumps was used to solvent delivery and a special cross-flow control. The separations were performed using a 10 kDa MW cutoff regenerated cellulose membrane in a 300 mm channel with 350  $\mu\text{m}$  thick spacer. The system is followed by a PN3242 4-channel UV-Vis/DAD detector and a 21-angle multiangle light scattering detector, MALS (PN3621). NovaFFF version 2.2.0.1 software was used to control the instruments, set separation parameters, collect data, handle signals from the detectors (MALS and DAD), and compute the radius and molar mass of particles during measurements. After samples were loaded into the AF4 channel, the separation process is performed in four steps: 1) Preset flow: The instrument enters the working state in advance according to the set experimental parameters, which is to ensure the stable state of the instrument and stabilize flows. 2) Focus step: During this step the sample is uploaded into the channel and compressed in a very narrow band by focus flow and cross-flow at the beginning of the channel and be pre-separated. 3) Elution: At this stage, the focus flow is released from the channel, and only the channel flow and the cross flow remains in the channel. The strength of hydrodynamic field applied to nanoparticles for their separation can be regulated by modifying the intensity of cross-flow while analytes elute along the channel towards the detectors. This parameter can be modified throughout

**TABLE 1 Method optimization for AuNPs analysis (Method 1-Gold nanoparticles, M1-G). All the experiment were conducted on PEG-AuNPs with a detector flow 0.5 ml/min, focus time 5 min, and mobile phase Milli-Q water.**

Methods	Crossflow-focus step (ml/min)	Initial crossflow-elution step (ml/min)	Final crossflow-elution step (ml/min)	Elution program	Duration (min)	Recovery (%)
M1-G	1	1.5	0	Linear	15	80.2
M2-G	1.5	2.0	0	Linear	15	79.6
M3-G	2.0	2.5	0	Linear	15	86.5
M4-G	2.5	3.0	0	Linear	15	90.5
M5-G	3.0	3.0	0	Linear	15	99.4

the analysis to generate a decreasing cross-flow (namely gradient). 4) Rinse step: The cross-flow is released at end of the separation process and the channel flow rinses the channel allowing for any remaining sample due to the cross-flow action to be removed.

For the method development, we conducted a two-stage optimization concerning crossflows and mobile phases to optimize sample recovery. Initially, the basic separation conditions were proposed by referring to relevant literatures (Schachermeyer et al., 2013; Ashby et al., 2014; Au - Drexel et al., 2020) with some adjustments. The main adjustments were the cross-flow rate in the focus step and the initial cross-flow rate in the elution step (Table 1). After that, considering the importance of mobile phase in the AF4 process and in the downstream applications of the analytes, different carrier compositions were studied: Milli-Q water, 10 mM Phosphate buffered saline, 10 mM Phosphate buffer, and 2 mM Citrate Buffer. The method was subjected to further optimization for the separation of AuNPs-BSA mixtures, by modification the cross-flow program during the elution step to achieve optimum separation for mixture components. The optimal separation parameters and the detailed optimization processes are illustrated in the discussion section.

### 3 Results and discussion

#### 3.1 Characterization of gold nanoparticles and AuNPs-BSA conjugates by batch sizing and UV-VIS spectroscopy

After synthesis, PEG- and Citrate-AuNPs were characterized by means of UV Spectroscopy and batch sizing.

Visually, PEG-AuNPs and Citrate-AuNPs appear as light red solutions. They are also clear and transparent without visible aggregation or precipitation, as shown in Figure 1, meaning they are stable colloids. For UV-Vis batch measurements, milli-Q water was used for background subtraction. The absorption spectra of both AuNPs displayed a surface plasmon resonance band at 525 nm (Figure 1), indicating that PEG-AuNPs and Citrate-AuNPs have very similar size and optical absorption properties.

Then, AuNPs were mixed with a solution of BSA and their UV profiles were re-evaluated. The spectra of both nanoparticles

showed a certain degree of red shift due to protein binding to AuNPs surface, which has been widely reported. (Liu et al., 2015).

A similar information is obtained through sizing, which at this day is the gold standard for evaluating nanoparticle conjugation. Dynamic light scattering (DLS) showed that freshly synthesized AuNPs averaged 38 and 25 nm respectively for PEG-AuNPs and Citrate-AuNPs (Figure 2). Following 30 min incubation with BSA, their size increased to 42 and 32 nm, indicating that BSA successfully coated AuNPs.

Based on the UV and DLS data, it is possible to confirm that there is an interaction between AuNPs and BSA, and that the system does not aggregate to a critical degree, a mechanism that would have red-shifted the signal more and yielded to a higher and more polydisperse size measurement. However, no information on the stoichiometry of conjugation can be obtained since the size distribution is not fully monodispersed, and the presence of free protein can hinder the measurement. The conjugates formed during this process would then need further purification and quantitative control to be further applied to biological detection and achieve quantification of analytes.

#### 3.2 AF4-multidetector

##### 3.2.1 Method development and characterization of AuNPs

The unique properties of gold nanoparticles are determined by the size of the nanoparticles and the action of surface stabilizer. (Bai et al., 2020). AF4 is a popular technique for sizing nanoparticles, which can be separated based on hydrodynamic diameter. Compared to other separation techniques it provides a gentle separation in native conditions and it is characterized by high flexibility in terms of mobile phase and injectable sample. Moreover, the retention time of AuNPs from fractogram can be directly correlated to the hydrodynamic diameter by Eq. 1.

$$d_h = 2kTVt_r / \eta\pi w^2 V_c \quad (1)$$

where  $k$  is the Boltzmann's constant ( $16 \text{ g cm}^2 \text{ s}^{-2} \text{ K}^{-1}$ ),  $T$  is absolute temperature (K),  $V$  is the channel flow rate ( $\text{cm}^3 \text{ s}^{-1}$ ),  $\eta$  is the carrier liquid viscosity ( $\text{g cm}^{-1} \text{ s}^{-1}$ ),  $w$  is the AF4 channel thickness (cm) and  $V_c$  is cross-flow rate ( $\text{cm}^3 \text{ s}^{-1}$ ). (Sánchez-Cachero et al., 2021)

Therefore, the retention time is affected by many factors, such as type of carrier liquid, membrane material, injection time, and cross flow rate, *etc.* (Saenmuangchin and Siripinyanond, 2018)

In this study, a 350  $\mu\text{m}$  thick spacer and a regenerated cellulose (RC) membrane (MWCO = 10 kDa) were used in agreement with earlier investigations. (Meisterjahn et al., 2014; Ramos et al., 2014; López-Sanz et al., 2019). According to reports, RC membrane has less hydrophobicity than polyethersulfone (PES), which is advantageous for the recovery of metallic NPs. (López-Heras et al., 2014). Another critical parameter is the injection time since it determines sample equilibration in the channel, critical for the complete separation of the sample in the subsequent elution process. (Gigault et al., 2014). Injection times from 3 to 5 min were selected for testing, both of which resulted in good separation between void peak and AuNPs (data not show). An injection time of 5 min was chosen to prevent the increase in equilibration time required for sample volume increases during method optimization. The cross-flow ( $V_c$ ) was studied according to AF4 theory: for a fixed spacer thickness and when the flow rate out of the channel ( $V_{out}$ ) remains constant (0.5 ml/min), retention time of species increase with the  $V_c/V_{out}$  ratio. (Bolea et al., 2011). Therefore, the cross-flow was tested from 1 to 3 ml/min using PEG-AuNPs (100 ppm) under the initial condition, as shown in Table 1.

Furthermore, considering that the synthesis conditions of AuNPs are carried out in an aqueous environment, we first used Milli-Q water as mobile phase. Of all methods, the best resolution between PEG-AuNPs and void peak was obtained for M5-G, as shown in Figure 3A, and gave us the smallest void peak and the best sample recovery (99.4%). Moreover, with M5-G, the Citrate-AuNPs (9.8 min) can also be successfully separated with 99.8% recovery and have different retention times than PEG-AuNPs (6.2 min).

We verified that both changes in AuNPs concentration (5–50  $\mu\text{g/ml}$ ) and AuNP injection volume (10–400  $\mu\text{l}$ ) allowed optimal recovery (97.8–100.5%). Method precision was assessed both on retention times and on signal intensity by performing

three independent injections of both NPs samples. The profiles exhibited deviations in terms of retention time and signal intensity <1%. The limit of detection (LOD) and quantification (LOQ) for AuNPs (expressed as mass of atomic Au) were calculated as the injected amount at which their specific signals (525 nm) are three or 10 times the signal noise of the baseline (Table 2).

Citrate-AuNPs (9.8 min) could be successfully separated from PEG-AuNPs and have different retention times than PEG-AuNPs (6.2 min).

Combining the results provided by DLS (Figure 2), we observed that though Citrate-AuNPs are hydrodynamically smaller than PEG ones they elute later (Figure 3B). The main reason for this phenomenon may be the stronger interactions between Citrate-AuNPs and the membrane which leads to delayed elution (Saenmuangchin and Siripinyanond, 2018). In terms of gyration radius ( $R_g$ ), measured by MALS, it was observed that both particles are highly monodispersed and have a very similar radius, i.e. 6.3 nm (Polydispersity Index PDI 1.006) for Citrate-AuNPs and 7.1 nm (PDI 1.013) for PEG-AuNPs. This value is lower than what observed for DLS measurements, and is consistent with the particles being solid spheres. In fact, their shape factor, expressed as the ratio between gyration and hydrodynamical radius ( $R_h$ ) (Marassi et al., 2018b; Marassi et al., 2021c), would equal to 0.6 when using the average DLS values, but to 0.75 when using the mode value. A value of 0.77 is expected for a compact sphere while a shape factor of 0.6/0.5 is typical for core-shell systems (Marassi et al., 2018a).

As a step forward, we considered the application envisioned for AuNPs and their conjugates, that require the shift towards buffers, and translated method optimization into a more representative medium as mobile phase. Indeed, the properties of the mobile phase (such as pH, ionic strength, and composition) directly influence the electrostatic properties of the AF4 system and samples. The choice of carrier composition needs to be taken into account on one side to improve the operational performance and on the other to ensure compatibility with the expected application and obtain representative results. (Gigault et al., 2014).

Firstly, a phosphate buffered saline solution (PBS, 10 mM, pH 7.4) was chosen as carrier for the separation of AuNPs. As shown in Figure 4, under the same separation conditions (Method 5-Gold nanoparticles, M5-G), the two AuNPs were extremely unstable in the channel: PEG-AuNPs aggregated and

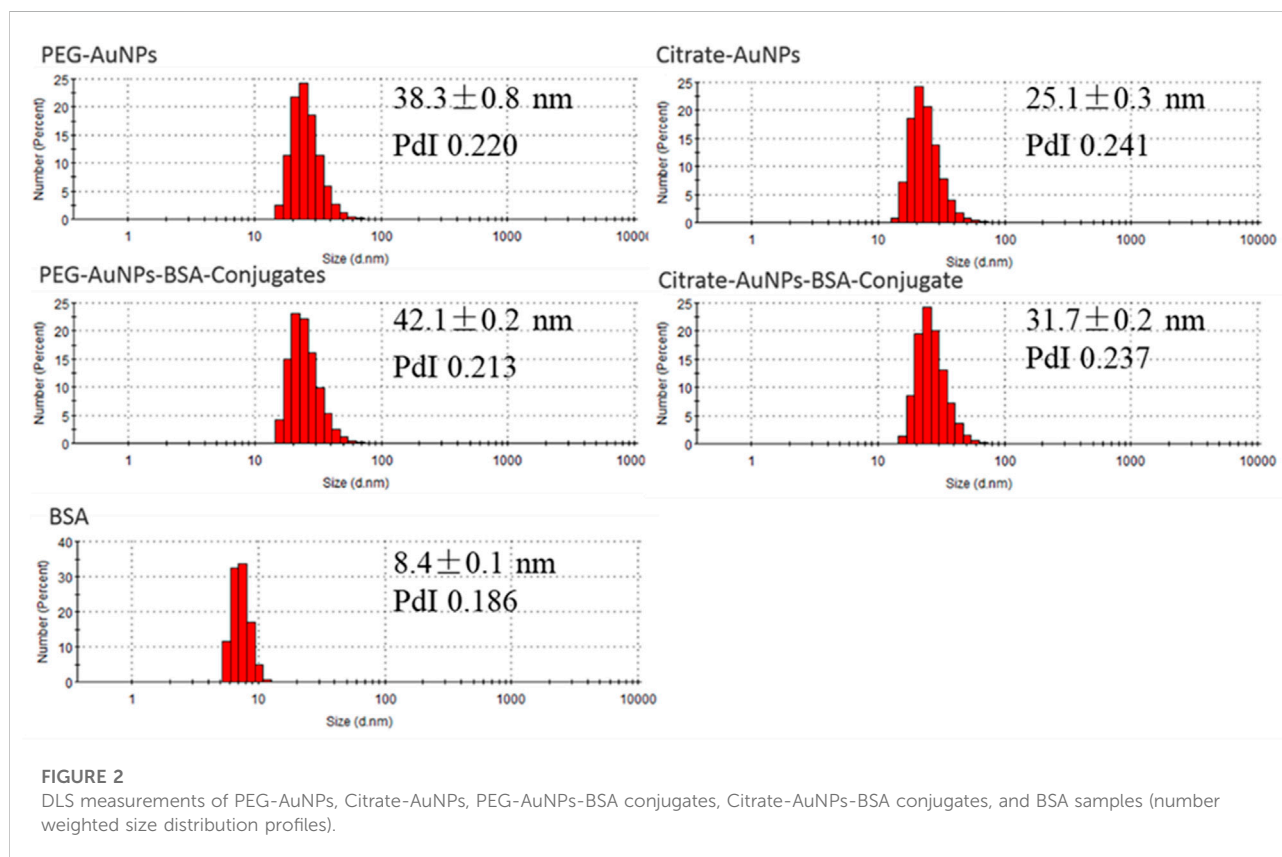
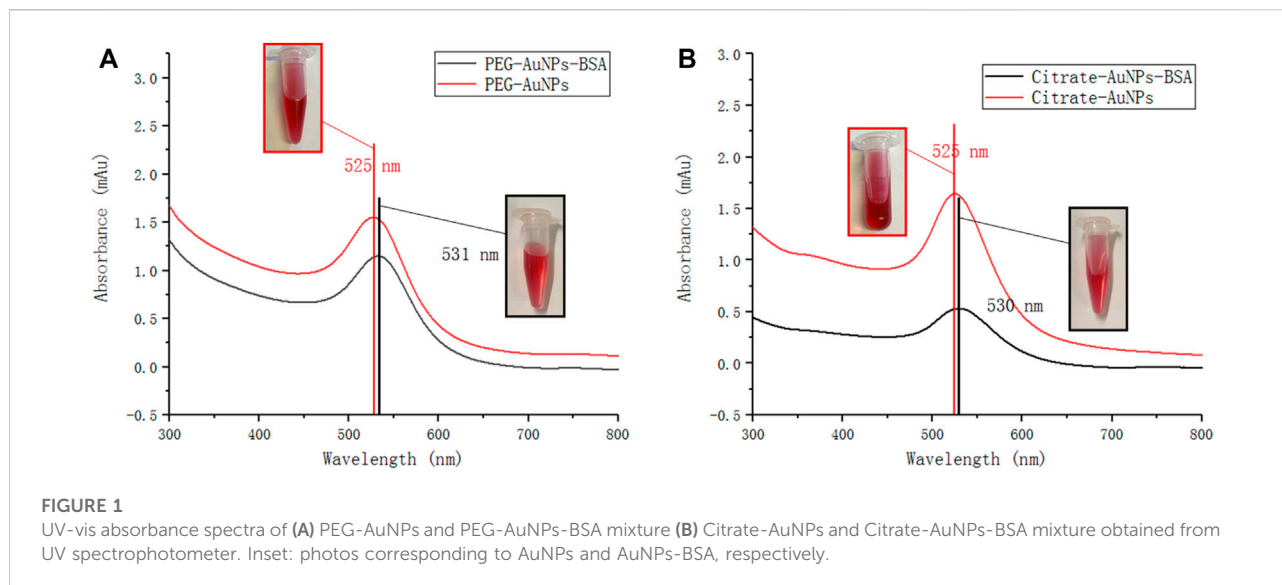
**TABLE 2** LOD and LOQ calculated values for AuNPs (expressed as atomic mass of Au) for the method M5-G with Milli-Q water as mobile phase.

Citrate-AuNPs (525 nm)		PEG-AuNPs (525 nm)	
LOD (ng)	LOQ (ng)	LOD (ng)	LOQ (ng)
5	15	1.6	5

**TABLE 3** State and recovery of samples derived by different mobile phase (Phosphate buffered saline PBS, Phosphate buffer PB, Citrate buffer CB). Aggregation: the sample remains in a colloidal state; Precipitation: the colloidal state of the sample is destroyed.

	Milli-Q water	PBS 10 mM pH 7.4	PB 10 mM pH 7.4	CB 2 mM pH 6.2
PEG-AuNPs	√Recovery 99.4%	√aggregation	√aggregation	√aggregation
Citrate-AuNPs	√Recovery 99.8%	×precipitation	×precipitation	×precipitation

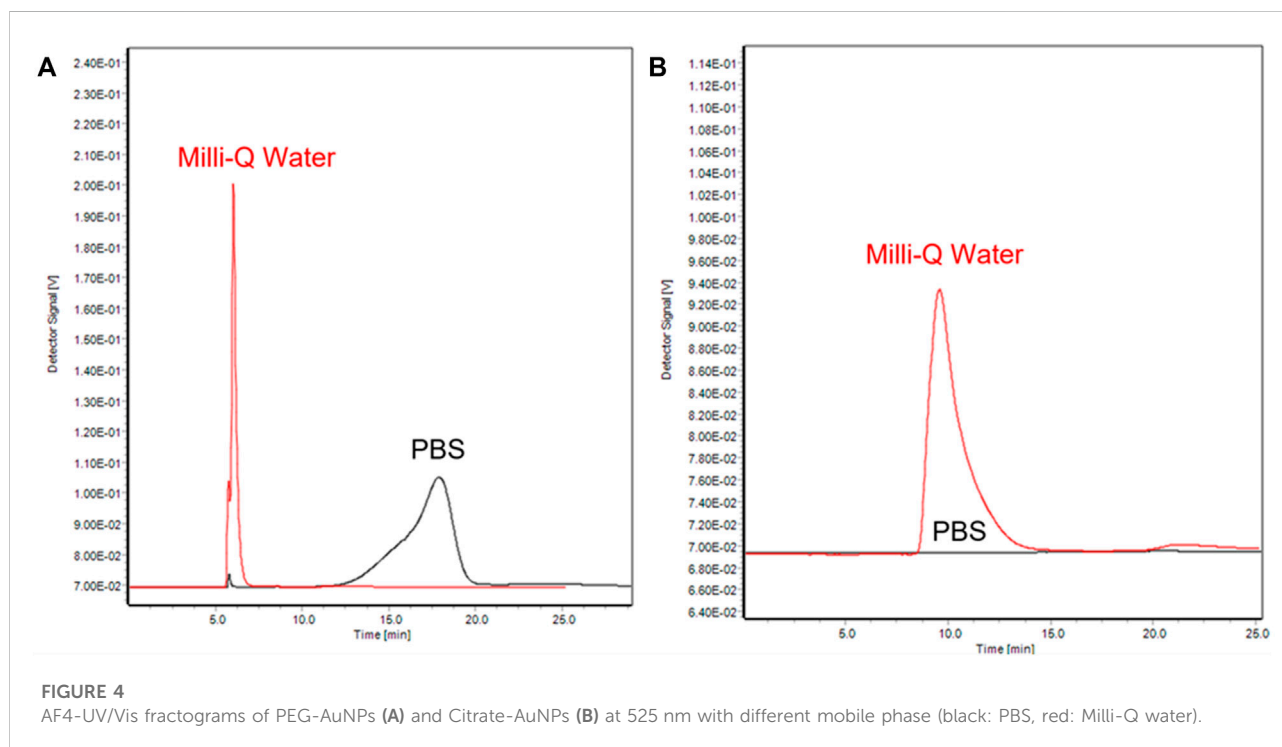
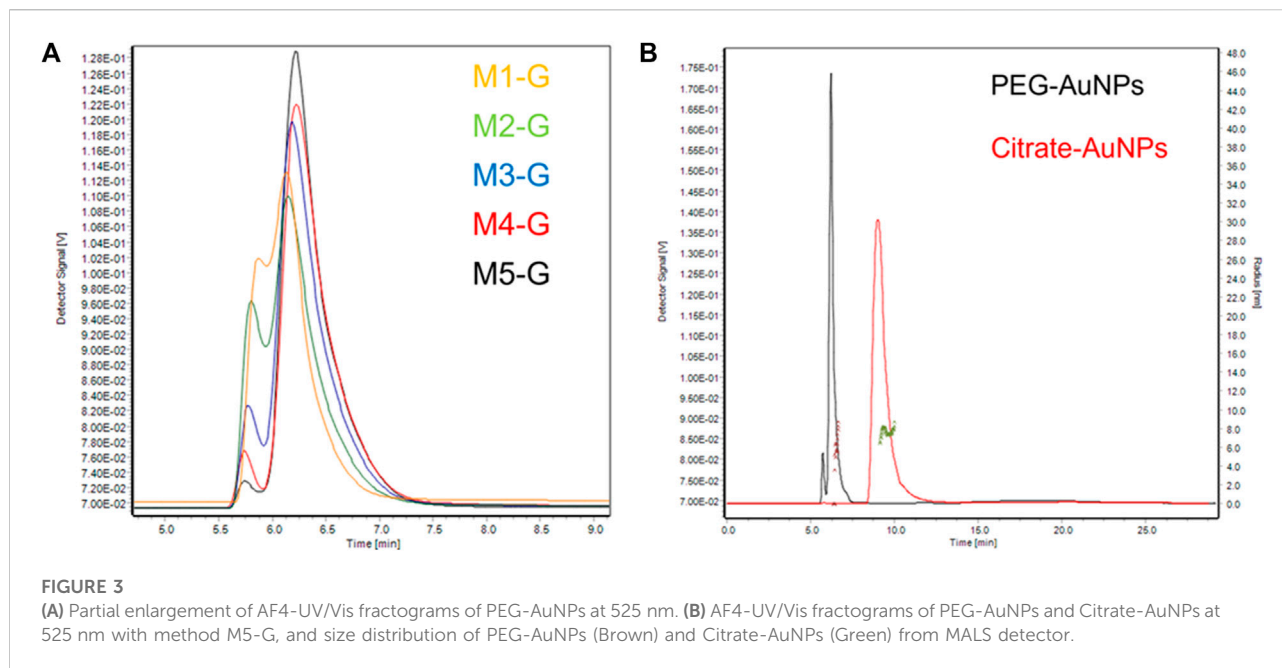




shifted to higher retention times (Figure 4A), while agglomeration occurs to Citrate-AuNPs which precipitates and cannot be eluted out of the channel (Figure 4B).

In addition, we tried several other different buffer solutions and evaluated elution results, as shown in Table 3.

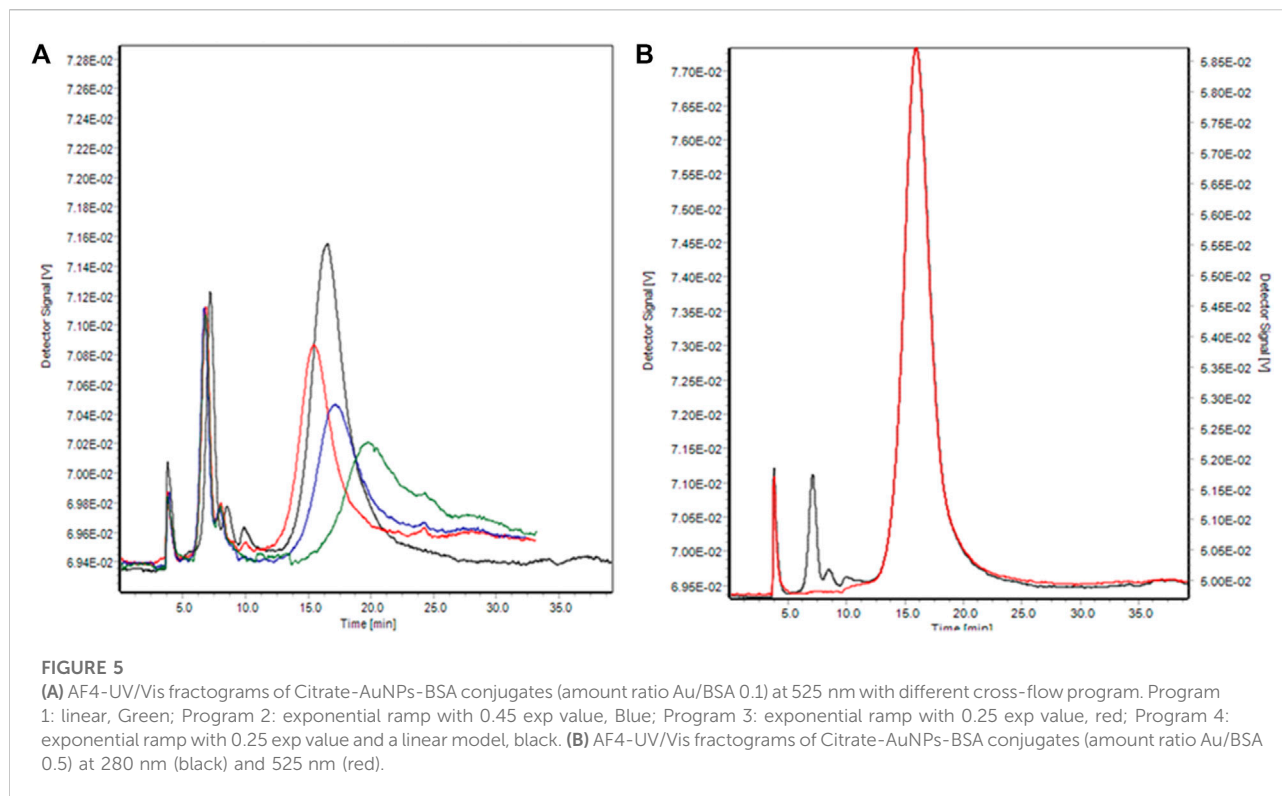
Citrate-AuNPs (characterized by bare surface) are subject to agglomeration and precipitation in the channel in all buffers and no elution peak is observed at 525 nm. Their colloidal state is thus destroyed. Contrarily, an elution peak is observed for PEG-AuNPs, highlighting that PEG protection



preserves the nanoparticles' colloidal state. However, the high ionic strength of the buffer is enough to still induce aggregation of the NPs.

To summarize, AuNPs alone will aggregate or even precipitate in the AF4 channel when increasing the ionic

strength of the mobile phase, that increases polydispersity and disrupts the colloidal properties of the nanoparticles. However, this does not mean that the synthesized AuNPs cannot be used in those buffers for further bio application. When proteins are present, they can promote a stable protein



corona formation on AuNPs surface, increase their stability and biocompatibility. Thus, we further evaluated and optimized separation parameters shifting from water to the application medium (e.g., PB) in the presence of BSA, to explore a complete and flexible analysis strategy monitoring the size evolution of synthesized and conjugated AuNPs. (Sermsri et al., 2010).

### 3.2.2 Method development and monitoring of AuNPs-BSA conjugation

Next, BSA was used as a model protein to progress method development, for its low price, high availability, and for its molar size placing between small chains like aptamers and bigger proteins such as antibodies. This approach aimed at building a flexible method able to be widely applied to also study other proteins and ligand adsorption behavior on gold nanoparticles surface, quantify and purify ready-to-use conjugated particles with improved quality for bio-detection. Conjugation was performed by mixing AuNPs and BSA in a 1:2 proportion in mass, to ensure BSA excess and avoid AuNP precipitation in the channel. The mixtures were injected after 30 min from mixing without pre-purification steps.

The initial separation conditions were those described in method M5-G (Table 1), using PB as carrier. The injection time was adjusted to 3 min, which was enough to separate the protein and the conjugates efficiently. The main adjustments to the elution program were made during the separation process. Several cross-flow programs in the elution step, which directly

**TABLE 4** Optimized method for the separation of BSA-AuNPs mixtures.

AF2000 operating conditions	
Detector flow (ml/min)	0.5
Cross flow (ml/min)	3.0 (0–9 min)
	3.0–0.4 (9–19 min, exp. 0.25)
	0.4–0.0 (19–34 min, linear)
	0.0 (34–39 min)
Injection flow (ml/min)	0.2
Injection time (min)	3.0

affected the elution efficiency of different components, were studied. Linear (Program 1, Figure 5A), exponential (Program 2 and 3, Figure 5A), and combinations of them were tested (Program 4, Figure 5A).

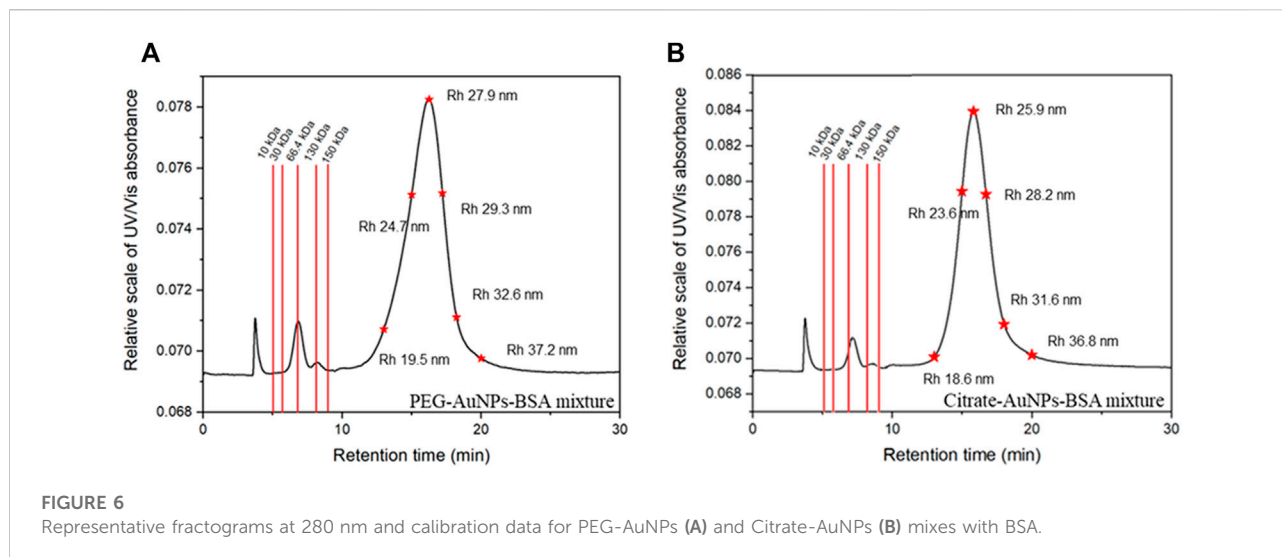
Overall, program four was considered as the best model and an additional linear elution stage was added to facilitate smooth elution of larger-sized conjugates. Under these optimal conditions (Table 4) we were able to successfully separate BSA, AuNPs, and conjugates. Moreover, the use of a multi-wavelength UV detector allowed to visualize selectively protein and AuNPs and easily assign the eluted peaks to the right component.

It is important to notice that though AuNPs are not stable in Phosphate buffer, in the presence of excess BSA they not only form conjugates products but also elute from the channel with excellent



**TABLE 5** LOD and LOQ calculated values for BSA and AuNPs (expressed as atomic mass of Au) for the optimized method described in **Table 4**.

BSA (280 nm)		Citrate-AuNPs (525 nm)		PEG-AuNPs (525 nm)	
LOD (pmol)	LOQ (pmol)	LOD (ng)	LOQ (ng)	LOD (ng)	LOQ (ng)
0.9	3	14	47	7	23



recovery (>97%). Last, method performance was evaluated through independent replicates for each Mix and BSA samples. The profiles exhibited a maximum of 0.5% and 1% deviation in terms of retention time and signal intensity. Higher shifts observed for the conjugate peaks between different BSA-AuNPs mixes are associated to different aggregation of the conjugates. The limit of detection (LOD) and quantification (LOQ) for BSA and AuNPs were calculated as described before from their respective specific signals (280 and 525 nm). The results are reported in **Table 5**.

The fractograms corresponding to the analysis of AuNP-BSA mixtures are shown in **Figure 6**. Peak attribution was performed both from MALS molar mass and size measurement and trough BSA injections.

BSA was eluted at 6.5 min: calculated MW for the BSA monomer was 65.9 kDa and its retention time was compatible with the one predicted by FFF theory; with respect to DLS measurements, FFF-calculated hydrodynamical radii resulted slightly higher for the conjugates, an effect justifiable by the lack of contribution from free BSA.

The second peak eluted after 15 min was indeed identified as the conjugate peak. The nature of the peak could also be confirmed by the high absorption at 525 nm (**Figure 5B**), which is only typical of AuNP and not relative to BSA.

The peak at 3 min (void time) observed in all fractograms was also observed for blank injections and thus was identified as a system peak. The optimized method provides enough separative

time and space to differentially elute analytes in a wide range of size (rh up to ~ 87 nm) in a reasonable time span. Moreover, it well separates the first eluting species (BSA) from its aggregates (dimer and trimer) and from the void peak.

**Figure 6A,B** report the calculated retentions time expected for proteins in a molar mass range of 10–200 kDa and for species with a hydrodynamic radius of 20–40 nm. This calculation easily show how proteins of different MW would be well separated both from the void and the conjugate peak, and how AuNP conjugates of different size could be successfully isolated. The developed method fulfills its scope of being adaptable to other conjugated systems exploiting different AuNPs and other kinds of proteins and ligands ranging from 10 to 200 kDa (ex. IgG ~ 140 kDa) and for the development of the assays of interest. It is also worth stressing out that since FFF is a gentle non-destructive technique a well separated protein peak allows also its collection; the collected protein is still not altered and pure and can be used for further experiment which is extremely important while working with expensive samples such as monoclonal antibodies or labeled proteins.

### 3.2.3 AuNPs-BSA characterization and insights on their conjugation mechanism

The detectors coupled at the end of the separative systems (DAD, MALS) allowed to record the continuous absorption spectrum and the Rg of the conjugates, which were monitored after 30 min of incubation and after 48h, to look for possible variations.

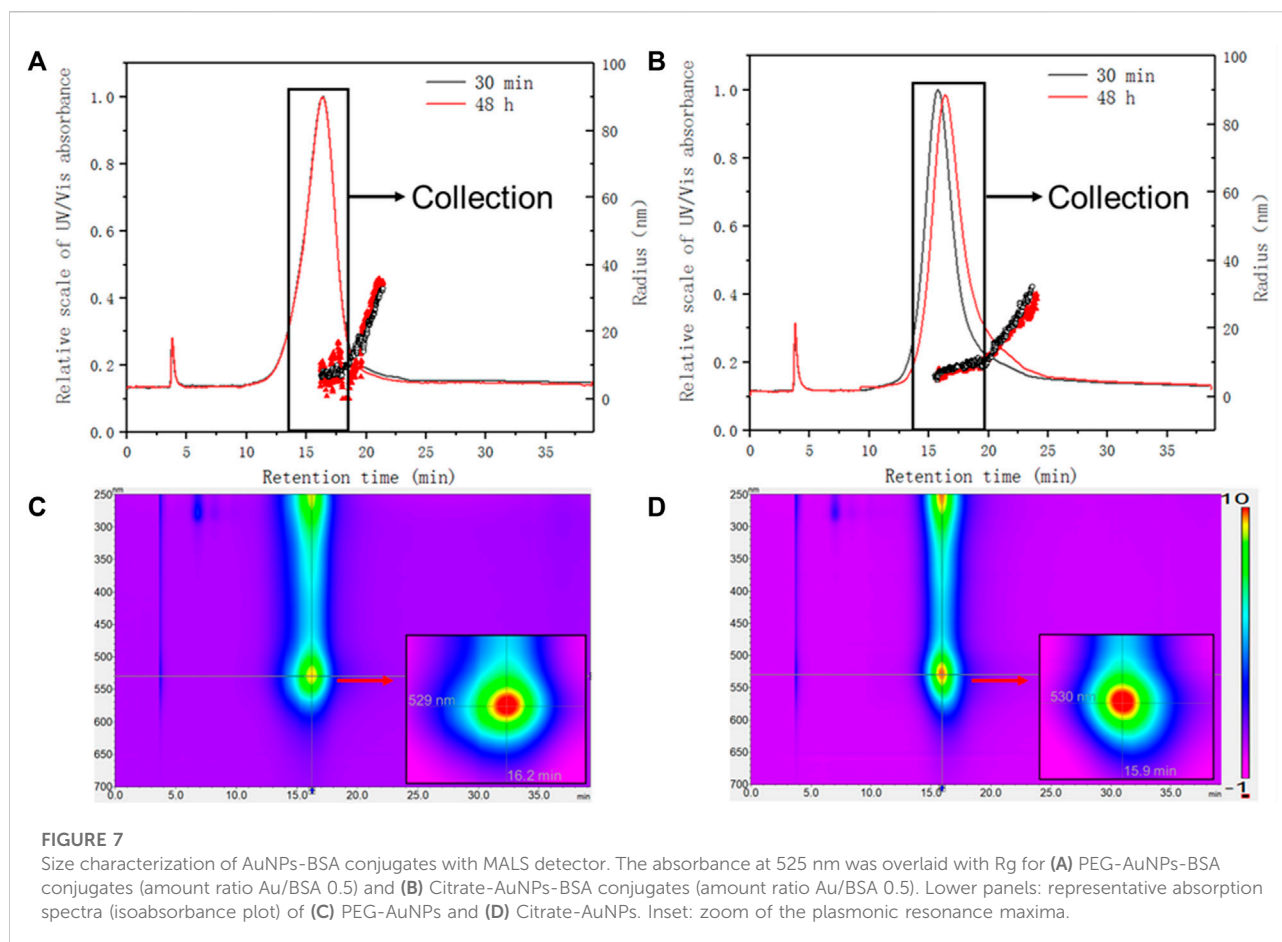


FIGURE 7

Size characterization of AuNPs-BSA conjugates with MALS detector. The absorbance at 525 nm was overlaid with Rg for (A) PEG-AuNPs-BSA conjugates (amount ratio Au/BSA 0.5) and (B) Citrate-AuNPs-BSA conjugates (amount ratio Au/BSA 0.5). Lower panels: representative absorption spectra (isoabsorbance plot) of (C) PEG-AuNPs and (D) Citrate-AuNPs. Inset: zoom of the plasmonic resonance maxima.

The size distribution and the absorption spectra for PEG-AuNPs-BSA and Citrate-AuNPs-BSA conjugates at different incubation time are shown in Figure 7.

In terms of UV absorption, both conjugates are similar in terms of plasmonic band (with a maximum at 529 nm and 530 nm respectively) and even after 48 h this trend did not change. When considering online sizing, two populations eluted within the main peak could be recognized in both cases: a monodispersed one, which consists of the majority of the conjugate, and a later eluting distribution with increasing size. PEG-AuNPs-BSA main population was found to be 9.5 nm in Rg (16.1–19.1 min), with a tail increasing from 11 to 34 nm (19.1–21.3 min). Citrate-AuNPs-BSA conjugates were also characterized by two populations, one with constant average Rg of 8.9 nm (15.4–20 min) and one with an increasing Rg ranging 11–30 nm (20–24 min).

The similar size distribution and fractogram at different incubation time indicates that both conjugates reached adsorption equilibrium within 30 min. After 48 h of incubation, the PEG conjugates showed a retention shift and loss of monodispersity, as shown in Figure 7A. Considering the surface properties of PEG-AuNPs, it may be caused by the insufficient binding between PEG and BSA during the

incubation, resulting in the shedding or aggregation of BSA. Instead, Citrate-AuNPs with bare surfaces have stronger affinity for BSA. This suggests that citrate-stabilized AuNPs could be a better candidate for protein conjugation.

The bigger populations observed for both conjugates (20–24 or 19.1–21.3 min) are not affected by visible changes during the incubation time, which indicates that they are formed during the interaction of AuNPs and BSA, and subsequent incubation did not change their binding behavior.

For both samples this population represents only a small part of the conjugate, and the area ratio of the two is 20:1. However, it represents impurities and would affect sensor performance and signal response, since it corresponds to uncontrolled conjugation: it is crucial to identify and remove it by means of fractionation. These aggregates may be associated to multiple BSAs combined with one AuNP, or AuNPs multimers bound to BSA, the latter being less likely since it would lead to a higher order of aggregation. If these species are not removed prior to the intended use of these particles misleading results may occur: e.g., in the case of colorimetric sensors with a target protein, the sensitivity would decrease in the first case (higher protein: AuNP ratio) or increase in the second case (higher AuNP: protein ratio). For the simple characterization of the species, we limited sample

consumption and injected 40  $\mu\text{l}$  (1  $\mu\text{g}$  Au), and by collecting 90% of the conjugate peak i.e. 2 min of elution, which both reduces dilution and selects monodisperse particles, the final concentration (expressed as  $\mu\text{g}$  of Au) of the purified conjugates is 0.9  $\mu\text{g}/\text{ml}$ . However, it is possible to scale up both injection volume and Au concentration at least by one order of magnitude respectively while retaining peak shape and separation quality, yielding fractions of purified conjugates of about 100  $\mu\text{g}/\text{ml}$ , more appealing for further use.

Finally, we considered the calculated size obtained by MALS for freshly, synthesized, AuNPs and their protein conjugates. MALS sizing in fact resulted the clearest in terms of PDI, and was less subject to interferences such as excess protein and membrane repulsion. This way, we evaluated the conjugation ratio between protein and AuNPs: this parameter is extremely relevant for biosensor development since it impacts reproducibility and quality. Moreover, the coexistence of different conjugations would have detrimental impact on sensor linearity and reliability. However, it is complex to achieve such a characterization with batch techniques or hydrodynamic sizing which is influenced by soft solvating layers, and this aspect is often left aside when dealing with particle conjugation. In our case, since we could isolate BSA-AuNPs without the compresence of BSA, which has a different retention time, we could directly and realistically measure the conjugate size. In particular, for both particles the radius of the conjugate between AuNPs and protein corresponded to the arithmetic sum between AuNPs and BSA monomer gyration radius.

In fact, for BSA-PEG-AuNPs the  $R_g$  was 9.5 nm (7+3) and for BSA-Citrate-AuNPs it was 8.9 nm (6+3). This information is useful to obtain the conjugation structure: since we had already calculated, from the shape factor, that AuNPs are spherical and compact, the addition of BSA (which is also a solid sphere or 3 nm  $R_g$ ) can lead to the sum of the original particles size only if the coating is uniform and a monolayer.

To summarize, through accurate method development and data evaluation, we managed to propose a flexible separation method, and obtained both data about the synthesis and conjugation quality, including considerations about the most stable AuNP, and the mechanism of conjugation, which involved formation of a uniform monolayer of BSA coating the gold particles. Our study involved for the first time the careful combination of FFF calibration through theoretical modelling, online detection and offline sizing, delivering a method which could be reliably applied to both different AuNPs and different conjugants in a wide molar mass range (10kDa–200 kDa). These results confirm how AF4-multidetector, when using an appropriate method, can be useful in all stages on conjugate preparation and can provide i. Starting material quality check; ii. Rapid characterization of conjugated species and evaluation of stability iii. Recovery of excess protein and fraction collection of monodispersed conjugated particles for improved sensing applications.

## 4 Conclusion

In our work, we broke through the limitations of traditional UV/Vis spectroscopy and DLS in the process of nanoparticle analysis and characterization, and combined the AF4-UV/Vis- MALS platform to explore the characterization of AuNPs with different surface properties and their conjugates. In order to apply AF4 for separation of AuNPs with various types of surface coating, we evaluated and optimized separation parameters shifting from water to the application medium. After method development, we successfully separated and characterized protein and conjugates. The developed method allows a fast purification of the analytes (BSA and BSA-AuNP) and their collection without altering their nature. The method exhibited high throughput and flexibility since it is possible to work with multiple kinds of AuNPs and proteins (10–200 kDa) with promising application as a powerful tool for the development, purification and quality monitoring of sensing components in bioassays. Moreover, the ability of AF4-UV/Vis-MALS platform for estimation of interaction of each type of AuNPs with BSA in is interesting and deserves further applications. The size information from MALS and DLS also revealed the combination ratio of AuNPs and BSA during the formation of conjugates, which is of great significance for the application of biological probes in the field of sensors.

## Data availability statement

The original contributions presented in the study are included in the article/supplementary material, further inquiries can be directed to the corresponding author.

## Author contributions

JW: Formal analysis, Methodology, Data curation, Writing—original draft. SG: Formal analysis, Writing—original draft. VM: Conceptualization, Formal analysis, Methodology, Writing—review and editing. BR: Resources, Writing—review and editing. PR: Funding acquisition, Writing—review and editing. AZ: Resources, Writing—review and editing.

## Funding

JW's grant was funded by the China Scholarship Council (CSC).

## Acknowledgments

We acknowledge prof Enrico Rampazzo for their support in performing DLS measurements.

## Conflict of interest

Authors VM, BR, PR and AZ are co-owners of ByFlow SRL.

The remaining authors declare that the research was conducted in the absence of any commercial or financial relationships that could be construed as a potential conflict of interest.

## References

- Ashby, J., Schachermeyer, S., Duan, Y., Jimenez, L. A., and Zhong, W. (2014). Probing and quantifying DNA–protein interactions with asymmetrical flow field-flow fractionation. *J. Chromatogr. A* 1358, 217–224. doi:10.1016/j.chroma.2014.07.002
- Au - Drexel, R., Au - Sogne, V., Au - Dinkel, M., Au - Meier, F., and Au - Klein, T. (2020). Asymmetrical flow field-flow fractionation for sizing of gold nanoparticles in suspension. *J. Vis. Exp.* (163), e61757. doi:10.3791/61757
- Bai, X., Wang, Y., Song, Z., Feng, Y., Chen, Y., Zhang, D., et al. (2020). The basic properties of gold nanoparticles and their applications in tumor diagnosis and treatment. *Int. J. Mol. Sci.* 21, 2480. doi:10.3390/ijms21072480
- Bolea, E., Jiménez-Lamana, J., Laborda, F., and Castillo, J. R. (2011). Size characterization and quantification of silver nanoparticles by asymmetric flow field-flow fractionation coupled with inductively coupled plasma mass spectrometry. *Anal. Bioanal. Chem.* 401 (9), 2723–2732. doi:10.1007/s00216-011-5201-2
- Boulos, S. P., Davis, T. A., Yang, J. A., Lohse, S. E., Alkilany, A. M., Holland, L. A., et al. (2013). Nanoparticle–protein interactions: A thermodynamic and kinetic study of the adsorption of bovine serum albumin to gold nanoparticle surfaces. *Langmuir* 29 (48), 14984–14996. doi:10.1021/la402920f
- Bouzas-Ramos, D., García-Alonso, J. I., Costa-Fernández, J. M., and Ruiz Encinar, J. (2019). Quantitative assessment of individual populations present in nanoparticle–antibody conjugate mixtures using AF4-ICP-MS/MS. *Anal. Chem.* 91 (5), 3567–3574. doi:10.1021/acs.analchem.8b05482
- Caputo, F., Mehn, D., Clogston, J. D., Rösslein, M., Prina-Mello, A., Borgos, S. E., et al. (2021). Asymmetric-flow field-flow fractionation for measuring particle size, drug loading and (in)stability of nanopharmaceuticals. The joint view of European Union Nanomedicine Characterization Laboratory and National Cancer Institute - nanotechnology Characterization Laboratory. *J. Chromatogr. A* 1635, 461767. doi:10.1016/j.chroma.2020.461767
- Chuang, Y.-C., Li, J.-C., Chen, S.-H., Liu, T.-Y., Kuo, C.-H., Huang, W.-T., et al. (2010). An optical biosensing platform for proteinase activity using gold nanoparticles. *Biomaterials* 31 (23), 6087–6095. doi:10.1016/j.biomaterials.2010.04.026
- Delong, R. K., Reynolds, C. M., Malcolm, Y., Schaeffer, A., Severs, T., and Wanekaya, A. (2010). Functionalized gold nanoparticles for the binding, stabilization, and delivery of therapeutic DNA, RNA, and other biological macromolecules. *Nanotechnol. Sci. Appl.* 3, 53–63. doi:10.2147/nsa.s8984
- Deng, Z. J., Mortimer, G., Schiller, T., Musumeci, A., Martin, D., and Minchin, R. F. (2009). Differential plasma protein binding to metal oxide nanoparticles. *Nanotechnology* 20 (45), 455101. doi:10.1088/0957-4484/20/45/455101
- Dobrovolskaia, M. A., Patri, A. K., Zheng, J., Clogston, J. D., Ayub, N., Aggarwal, P., et al. (2009). Interaction of colloidal gold nanoparticles with human blood: Effects on particle size and analysis of plasma protein binding profiles. *Nanomedicine Nanotechnol. Biol. Med.* 5 (2), 106–117. doi:10.1016/j.nano.2008.08.001
- Fernández-López, C., Mateo-Mateo, C., Álvarez-Puebla, R. A., Pérez-Juste, J., Pastoriza-Santos, I., and Liz-Marzán, L. M. (2009). Highly controlled silica coating of PEG-capped metal nanoparticles and preparation of SERS-encoded particles. *Langmuir* 25 (24), 13894–13899. doi:10.1021/la9016454
- Free, P., Shaw, C. P., and Lévy, R. (2009). PEGylation modulates the interfacial kinetics of proteases on peptide-capped gold nanoparticles. *Chem. Commun.* 33, 5009–5011. doi:10.1039/b910657j
- Gigault, J., Pettibone, J. M., Schmitt, C., and Hackley, V. A. (2014). Rational strategy for characterization of nanoscale particles by asymmetric-flow field flow fractionation: A tutorial. *Anal. Chim. Acta* 809, 9–24. doi:10.1016/j.aca.2013.11.021
- Guarise, C., Pasquato, L., De Filippis, V., and Scrimin, P. (2006). Gold nanoparticles-based protease assay. *Proc. Natl. Acad. Sci. U. S. A.* 103 (11), 3978–3982. doi:10.1073/pnas.0509372103
- Jamkhande, P. G., Ghule, N. W., Bamer, A. H., and Kalaskar, M. G. (2019). Metal nanoparticles synthesis: An overview on methods of preparation, advantages and disadvantages, and applications. *J. Drug Deliv. Sci. Technol.* 53, 101174. doi:10.1016/j.jddst.2019.101174
- Lee, J. H., Yang, J. S., Lee, S.-H., and Moon, M. H. (2018). Analysis of lipoprotein-specific lipids in patients with acute coronary syndrome by asymmetrical flow field-flow fractionation and nanoflow liquid chromatography-tandem mass spectrometry. *J. Chromatogr. B* 1099, 56–63. doi:10.1016/j.jchromb.2018.09.016
- Leeman, M., Albers, W. M., Bombera, R., Kuncova-Kallio, J., Tuppurainen, J., and Nilsson, L. (2021). Asymmetric flow field-flow fractionation coupled to surface plasmon resonance detection for analysis of therapeutic proteins in blood serum. *Anal. Bioanal. Chem.* 413 (1), 117–127. doi:10.1007/s00216-020-03011-x
- Leeman, M., Choi, J., Hansson, S., Storm, M. U., and Nilsson, L. (2018). Proteins and antibodies in serum, plasma, and whole blood-size characterization using asymmetrical flow field-flow fractionation (AF4). *Anal. Bioanal. Chem.* 410 (20), 4867–4873. doi:10.1007/s00216-018-1127-2
- Li, L., Mu, Q., Zhang, B., and Yan, B. (2010). Analytical strategies for detecting nanoparticle–protein interactions. *Analyst* 135 (7), 1519–1530. doi:10.1039/c0an00075b
- Liu, F., Wang, L., Wang, H., Yuan, L., Li, J., Brash, J. L., et al. (2015). Modulating the activity of protein conjugated to gold nanoparticles by site-directed orientation and surface density of bound protein. *ACS Appl. Mat. Interfaces* 7 (6), 3717–3724. doi:10.1021/am5084545
- López-Heras, I., Madrid, Y., and Cámara, C. (2014). Prospects and difficulties in TiO<sub>2</sub> nanoparticles analysis in cosmetic and food products using asymmetrical flow field-flow fractionation hyphenated to inductively coupled plasma mass spectrometry. *Talanta* 124, 71–78. doi:10.1016/j.talanta.2014.02.029
- López-Sanz, S., Fariñas, N. R., Martín-Doimeadios, R. d. C. R., and Ríos, Á. (2019). Analytical strategy based on asymmetric flow field flow fractionation hyphenated to ICP-MS and complementary techniques to study gold nanoparticles transformations in cell culture medium. *Anal. Chim. Acta X* 1053, 178–185. doi:10.1016/j.aca.2018.11.053
- Lundqvist, M., Stigler, J., Elia, G., Lynch, I., Cedervall, T., and Dawson, K. A. (2008). Nanoparticle size and surface properties determine the protein corona with possible implications for biological impacts. *Proc. Natl. Acad. Sci. U. S. A.* 105 (38), 14265–14270. doi:10.1073/pnas.0805135105
- Marassi, V., Beretti, F., Roda, B., Alessandrini, A., Facci, P., Maraldi, T., et al. (2019). A new approach for the separation, characterization and testing of potential prionoid protein aggregates through hollow-fiber flow field-flow fractionation and multi-angle light scattering. *Anal. Chim. Acta* 1087, 121–130. doi:10.1016/j.aca.2019.08.003
- Marassi, V., Calabria, D., Trozzi, I., Zattoni, A., Reschiglian, P., and Roda, B. (2021). Comprehensive characterization of gold nanoparticles and their protein conjugates used as a label by hollow fiber flow field flow fractionation with photodiode array and fluorescence detectors and multiangle light scattering. *J. Chromatogr. A* 1636, 461739. doi:10.1016/j.chroma.2020.461739
- Marassi, V., Casolari, S., Panzavolta, S., Bonvicini, F., Gentilomi, G. A., Giordani, S., et al. (2022). Synthesis monitoring, characterization and cleanup of Ag-polydopamine nanoparticles used as antibacterial agents with field-flow fractionation. *Antibiotics* 11, 358. doi:10.3390/antibiotics11030358
- Marassi, V., De Marchis, F., Roda, B., Bellucci, M., Capecci, A., Reschiglian, P., et al. (2021). Perspectives on protein biopolymers: Miniaturized flow field-flow fractionation-assisted characterization of a single-cysteine mutated phaseolin expressed in transplastomic tobacco plants. *J. Chromatogr. A* 1637, 461806. doi:10.1016/j.chroma.2020.461806
- Marassi, V., Di Cristo, L., Smith, S. G. J., Ortelli, S., Blosi, M., Costa, A. L., et al. (2018). Silver nanoparticles as a medical device in healthcare settings: A five-step approach for candidate screening of coating agents. *R. Soc. open Sci.* 5 (1), 171113. doi:10.1098/rsos.171113

## Publisher's note

All claims expressed in this article are solely those of the authors and do not necessarily represent those of their affiliated organizations, or those of the publisher, the editors and the reviewers. Any product that may be evaluated in this article, or claim that may be made by its manufacturer, is not guaranteed or endorsed by the publisher.



- Marassi, V., Giordani, S., Reschiglian, P., Roda, B., and Zattoni, A. (2022). Tracking heme-protein interactions in healthy and pathological human serum in native conditions by miniaturized FFF-multidetector. *Appl. Sci.* 12, 6762. doi:10.3390/app12136762
- Marassi, V., Macis, M., Giordani, S., Ferrazzano, L., Tolomelli, A., Roda, B., et al. (2022). Application of af4-multidetector to liraglutide in its formulation: Preserving and representing native aggregation. *Molecules* 27, 5485. doi:10.3390/molecules27175485
- Marassi, V., Maggio, S., Battistelli, M., Stocchi, V., Zattoni, A., Reschiglian, P., et al. (2021). FFF-based high-throughput sequence shortlisting to support the development of aptamer-based analytical strategies. *Anal. Bioanal. Chem.* 414 (18), 5519–5527. doi:10.1007/s00216-022-03971-2
- Marassi, V., Roda, B., Casolari, S., Ortelli, S., Blosi, M., Zattoni, A., et al. (2018). Hollow-fiber flow field-flow fractionation and multi-angle light scattering as a new analytical solution for quality control in pharmaceutical nanotechnology. *Microchem. J.* 136, 149–156. doi:10.1016/j.microc.2016.12.015
- Mariam, J., Dongre, P. M., and Kothari, D. C. (2011). Study of interaction of silver nanoparticles with bovine serum albumin using fluorescence spectroscopy. *J. Fluoresc.* 21 (6), 2193–2199. doi:10.1007/s10895-011-0922-3
- Meisterjahn, B., Neubauer, E., Von der Kammer, F., Hennecke, D., and Hofmann, T. (2014). Asymmetrical flow-field-flow fractionation coupled with inductively coupled plasma mass spectrometry for the analysis of gold nanoparticles in the presence of natural nanoparticles. *J. Chromatogr. A* 1372, 204–211. doi:10.1016/j.chroma.2014.10.093
- Melikishvili, S., Piovarci, I., and Hianik, T. (2021). Advances in colorimetric assay based on AuNPs modified by proteins and nucleic acid aptamers. *Chemosensors*. doi:10.3390/chemosensors9100281
- Nicoară, R., Ilieș, M., Uifălean, A., Iuga, C. A., and Loghin, F. (2019). Quantification of the PEGylated gold nanoparticles protein corona. Influence on nanoparticle size and surface chemistry. *Appl. Sci.* 9, 4798. doi:10.3390/app9224789
- Piovarci, I., Melikishvili, S., Tatarko, M., Hianik, T., and Thompson, M. (2021). Detection of sub-nanomolar concentration of trypsin by thickness-shear mode acoustic biosensor and spectrophotometry. *Biosensors* 11, 117. doi:10.3390/bios11040117
- Qureshi, R. N., and Kok, W. T. (2011). Application of flow field-flow fractionation for the characterization of macromolecules of biological interest: A review. *Anal. Bioanal. Chem.* 399 (4), 1401–1411. doi:10.1007/s00216-010-4278-3
- Ramos, K., Ramos, L., Cámara, C., and Gómez-Gómez, M. M. (2014). Characterization and quantification of silver nanoparticles in nutraceuticals and beverages by asymmetric flow field flow fractionation coupled with inductively coupled plasma mass spectrometry. *J. Chromatogr. A* 1371, 227–236. doi:10.1016/j.chroma.2014.10.060
- Roda, B., Marassi, V., Zattoni, A., Borghi, F., Anand, R., Agostoni, V., et al. (2018). Flow field-flow fractionation and multi-angle light scattering as a powerful tool for the characterization and stability evaluation of drug-loaded metal-organic framework nanoparticles. *Anal. Bioanal. Chem.* 410 (21), 5245–5253. doi:10.1007/s00216-018-1176-6
- Saenmuangchin, R., and Siripinyanond, A. (2018). Flow field-flow fractionation for hydrodynamic diameter estimation of gold nanoparticles with various types of surface coatings. *Anal. Bioanal. Chem.* 410 (26), 6845–6859. doi:10.1007/s00216-018-1284-3
- Safenkova, I. V., Zherdev, A. V., and Dzantiev, B. B. (2010). Correlation between the composition of multivalent antibody conjugates with colloidal gold nanoparticles and their affinity. *J. Immunol. Methods* 357 (1), 17–25. doi:10.1016/j.jim.2010.03.010
- Sánchez-Cachero, A., López-Sanz, S., Fariñas, N. R., Ríos, Á., and Martín-Doimeadios, R. d. C. R. (2021). A method based on asymmetric flow field flow fractionation hyphenated to inductively coupled plasma mass spectrometry for the monitoring of platinum nanoparticles in water samples. *Talanta* 222, 121513. doi:10.1016/j.talanta.2020.121513
- Schachermeyer, S., Ashby, J., and Zhong, W. (2013). Aptamer-protein binding detected by asymmetric flow field flow fractionation. *J. Chromatogr. A* 1295, 107–113. doi:10.1016/j.chroma.2013.04.063
- Sermisri, W., Jarujamrus, P., Shiowatana, J., Siripinyanond, A. J. A., and Chemistry, B. (2010). Flow field-flow fractionation: A versatile approach for size characterization of  $\alpha$ -tocopherol-induced enlargement of gold nanoparticles. *Anal. Bioanal. Chem.* 396, 3079–3085. doi:10.1007/s00216-010-3511-4
- Tian, L., Chang, A., and Melancon, M. P. (2017). Exploring gold nanoparticle interactions with proteins and the tumor microenvironment in biological systems. *Transl. Cancer Res.* 6 (2), S309–s312. doi:10.21037/tcr.2017.03.53
- Treuel, L., Malissek, M., Gebauer, J. S., and Zellner, R. (2010). The influence of surface composition of nanoparticles on their interactions with serum albumin. *ChemPhysChem* 11 (14), 3093–3099. doi:10.1002/cphc.201000174
- Tsai, D.-H., DelRio, F. W., Keene, A. M., Tyner, K. M., MacCuspie, R. I., Cho, T. J., et al. (2011). Adsorption and conformation of serum albumin protein on gold nanoparticles investigated using dimensional measurements and *in situ* spectroscopic methods. *Langmuir* 27 (6), 2464–2477. doi:10.1021/la104124d
- Ventouri, I. K., Loeber, S., Somsen, G. W., Schoenmakers, P. J., and Astefanei, A. (2022). Field-flow fractionation for molecular-interaction studies of labile and complex systems: A critical review. *Anal. Chim. Acta* 1193, 339396. doi:10.1016/j.aca.2021.339396
- Wang, L., Li, S., Yin, J., Yang, J., Li, Q., Zheng, W., et al. (2020). The density of surface coating can contribute to different antibacterial activities of gold nanoparticles. *Nano Lett.* 20 (7), 5036–5042. doi:10.1021/acs.nanolett.0c01196
- Wimuktiwan, P., Shiowatana, J., and Siripinyanond, A. (2015). Investigation of silver nanoparticles and plasma protein association using flow field-flow fractionation coupled with inductively coupled plasma mass spectrometry (FFF-ICP-MS). *J. Anal. At. Spectrom.* 30 (1), 245–253. doi:10.1039/c4ja00225c
- Yang, K., Hu, Y., and Dong, N. (2016). A novel biosensor based on competitive SERS immunoassay and magnetic separation for accurate and sensitive detection of chloramphenicol. *Biosens. Bioelectron.* X, 80, 373–377. doi:10.1016/j.bios.2016.01.064
- Zappi, A., Marassi, V., Kassouf, N., Giordani, S., Pasqualucci, G., Garbini, D., et al. (2022). A green analytical method combined with chemometrics for traceability of tomato sauce based on colloidal and volatile fingerprinting. *Molecules* 27, 5507. doi:10.3390/molecules27175507
- Zhang, F., and Liu, J. (2021). Label-free colorimetric biosensors based on aptamers and gold nanoparticles: A critical review. *Anal. Sens.* 1 (1), 30–43. doi:10.1002/ans.202000023